THE JOURNAL OF PHYSICAL CHEMISTRY C

Article

pubs.acs.org/JPCC

Comparing the Pressure-Induced Structural Behavior of $CuCr_2O_4$ and $CuCr_2Se_4$ Spinels

I. Efthimiopoulos,*[,†,‡] V. Tsurkan,[§,∥] A. Loidl,[∥] Dongzhou Zhang,[⊥] and Y. Wang*[,†]

[†]Department of Physics, Oakland University, Rochester, Michigan 48309, United States

[‡]Deutsches GeoForschungsZentrum (GFZ), Section 4.3, Telegrafenberg, 14473 Potsdam, Germany

[§]Institute of Applied Physics, Academy of Sciences of Moldova, MD 2028 Chisinau, Republic of Moldova

[∥]Experimental Physics 5, Center for Electronic Correlations and Magnetism, Institute of Physics, University of Augsburg, D-86159 Augsburg, Germany

[⊥]Partnership for Extreme Crystallography, University of Hawaii at Manoa, Honolulu, Hawaii 96822, United States

Supporting Information

ABSTRACT: We have conducted high-pressure measurements on the $CuCr_2O_4$ and $CuCr_2Se_4$ spinels to unravel the structural systematics of these materials under compression. Our studies have revealed diverse structural behavior in these two compounds. In particular, $CuCr_2O_4$ retains its ambient-pressure $I4_1/amd$ structure up to 50 GPa. Close inspection of the lattice and interatomic parameters reveals a compressibility change near 23 GPa, which is accompanied by an expansion of the apical Cr−O bond distances. We speculate that an outer Cr^{3+} 3d orbital reorientation might be at play in this system, manifesting as the change in compressibility at that pressure point. On the other hand, $CuCr_2Se_4$ undergoes a structural transformation from the starting $Fd\bar{3}m$ phase toward a monoclinic structure initiated at ∼8 GPa and completed at ∼20 GPa. This high-pressure behavior resembles that of $ZnCr_2Se_4$, and it appears that, unlike similar chalcogenide Cr spinels, steric effects take a leading role in this pressure-induced $Fd\bar{3}m$ → monoclinic transition. Close comparison of our results with the reported literature yields significant insights behind the pressure-induced structural systematics of this important family of materials, thus both allowing for the careful manipulation of the structural/physical properties of these systems by strain and promoting our understanding of similar pressure-induced effects in relevant systems.

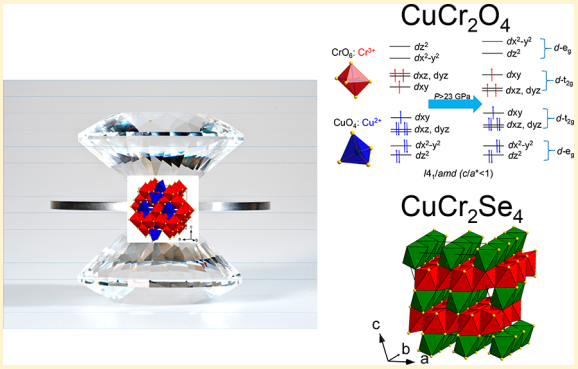

1. INTRODUCTION

The series of Cr-bearing compounds with stoichiometry $A^{2+}Cr^{3+}{}_2X^{2-}{}_4$ (A^{2+} = Mn−Zn, Cd, Hg; X^{2-} = O, S, Se) crystallize in three diverse structures at ambient conditions, depending on the constituent elements A and X.[1−3] The majority of the Cr-bearing oxide members of this series adopt either a cubic spinel phase (space group (SG) $Fd\bar{3}m$, Z = 8, Figure 1) or a tetragonal modification of this cubic spinel structure due to strong Jahn−Teller effects (SG $I4_1/amd$, Z = 4, Figure 1).[4] The latter tetragonal phase is a direct subgroup of SG $Fd\bar{3}m$[4], with the c-axis in the two structures being common, whereas the tetragonal a_{tetr}-axis equals the cubic lattice parameter a_{cub} divided by $2^{1/2}$ (Figure 1). Furthermore, due to the tetragonal symmetry, the Cr−X−Cr, Cr−X, and Cr−Cr parameters split into two components, an apical component (along the c-axis) and an equatorial component (parallel to the ab-plane); the A−X bond distance remains unique. Both of these structures are composed of AX_4 tetrahedral and edge-sharing CrX_6 octahedral units. In addition, due to the geometric frustration of the magnetic Cr^{3+} cations residing in a pyrochlore lattice, the spinel structure has been considered as a key system for studying magnetic exchange interactions in solids.[5,6]

The third structure adopted by several $A^{2+}Cr^{3+}{}_2X^{2-}{}_4$ chalcogenides is the monoclinic Cr_3S_4-type phase (SG $C2/m$, Z = 2), which can be viewed as a defect variant of the hexagonal NiAs-type structure with ordered vacancies.[7] Both types of cations, A^{2+} and Cr^{3+}, are octahedrally coordinated with respect to the anions in this phase, and because the Cr_3S_4-type structure has a higher density than the spinel one, this monoclinic Cr_3S_4-type phase can be viewed as a high-pressure polymorph of the spinels of this series. Indeed, high pressure and/or high temperature has been used to transform several thiospinels into this denser Cr_3S_4-type phase.[8,9] These structural transitions are also accompanied by significant alterations in the magnetic and electronic properties.[2,10]

Nevertheless, the high-pressure modification appears to depend critically on the type of A cation and the anion in

Received: May 15, 2017
Revised: July 11, 2017
Published: July 12, 2017

DOI: 10.1021/acs.jpcc.7b04657
J. Phys. Chem. C 2017, 121, 16513−16520

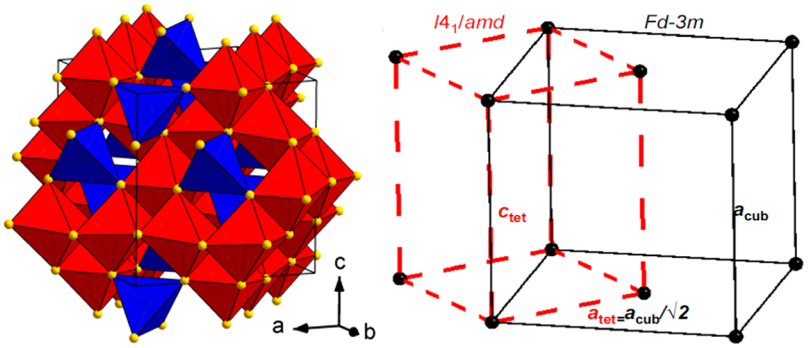

Figure 1. Polyhedral representation of the ambient-pressure spinel structure (SG $Fd\bar{3}m$, Z = 8, left). The blue and red polyhedra correspond to $CuSe_4$ and $CrSe_6$ units. The Se anions are displayed as yellow spheres. The geometrical relationship between the unit cells of $Fd\bar{3}m$ (solid black lines) and $I4_1/amd$ (dashed red lines) structures is also displayed.

Cr-bearing spinels. For example, $ZnCr_2O_4$ adopts an orthorhombic phase at 30 GPa,[11] $ZnCr_2S_4$ undergoes two successive structural transitions at 22 GPa ($Fd\bar{3}m \rightarrow I4_1/amd$) and at 33 GPa ($I4_1/amd \rightarrow$ orthorhombic),[12] and $ZnCr_2Se_4$ transforms into a monoclinic $CrMo_2S_4$-type structure (a superstructure of the Cr_3S_4-type phase) above 15 GPa;[13] for direct comparison with the latter, $CdCr_2Se_4$ undergoes an $Fd\bar{3}m \rightarrow I4_1/amd$ transition at 11 GPa.[14] Consequently, it becomes imperative to understand the influence of the constituent ions in the pressure-induced structural behavior of these Cr-based materials to elucidate in depth the stress–structure relationship. The latter is crucial knowledge for thin film applications, since the lattice mismatch between the film and the underlying substrate always introduces compressive/tensile strain at the interface, which can in turn modify the physical properties of the film.[15]

Among the various Cr-bearing spinels, the $CuCr_2X_4$ series (X = O, S, Se) stands out due to the substantial divergence in physical properties. In particular, $CuCr_2O_4$ is an insulating ferrimagnet and crystallizes in a tetragonal $I4_1/amd$ structure at ambient conditions, due to the Jahn–Teller active Cu^{2+} cation (Figure 1).[16] This Jahn–Teller distortion is suppressed above 870 K,[17] whereas cooling leads to a coupled magnetostructural transition into a ferrimagnetic orthorhombic phase at 135 K.[18−20] On the other hand, both $CuCr_2S_4$ and $CuCr_2Se_4$ adopt the cubic $Fd\bar{3}m$ structure and are itinerant ferromagnets. The exact valence state of copper and the origin behind the magnetic properties of these two compounds have been debated for several decades. The currently accepted model involves a hole-mediated magnetic exchange between the localized electrons of Cr^{3+} and delocalized holes from the Se 4p states, with the Cu cations exhibiting both monovalent and divalent valence states.[21−23] In addition, $CuCr_2Se_4$ has the highest Curie temperature among Cr-bearing spinels (T_C = 415 K),[24] thus making it appealing for use in magnetic devices.[25]

This significant diversity in physical properties makes $CuCr_2O_4$ and $CuCr_2Se_4$ ideal systems for comparing the effect of the anion alone on the pressure-induced structural evolution. As we shall discuss later, however, the A cations also plays a crucial part in the structural properties under pressure. To date, the only pressure-related studies on these two compounds have dealt with the pressure dependence of T_C.[24,26] In particular, the rate of pressure change was dT_C/dP = −4.1 K/GPa, and dT_C/dP = +1.6−2 K/GPa for $CuCr_2Se_4$ and $CuCr_2O_4$, respectively;[24,26] no structural data have been reported. Furthermore, a single-crystal X-ray diffraction (XRD) study on a natural $CuCr_{1.7}V_{0.3}S_4$ sample did not indicate any structural transition up to 7 GPa.[27]

Our high-pressure powder XRD studies have revealed a divergence in the structural behavior of the two materials under compression. In particular, $CuCr_2O_4$ retains its starting $I4_1/amd$ structure up to 50 GPa, with evidence of a second-order isostructural transition between 24 and 30 GPa. On the other hand, $CuCr_2Se_4$ adopts a monoclinic $CrMo_2S_4$-type structure above ∼8 GPa, similar to $ZnCr_2Se_4$,[13] with further compression up to 40 GPa leading apparently toward a high-symmetry disordered phase. This divergence in the high-pressure structural behavior illustrates the significant effect of the anions on the pressure-induced structural transformations of these compounds.

2. EXPERIMENTAL SECTION

The synthetic single-crystalline $CuCr_2O_4$ and $CuCr_2Se_4$ samples were ground into a fine powder for performing the angle-resolved high-pressure powder XRD experiments. Details of the synthesis have been reported elsewhere.[28] The high-pressure sample environment was generated by a rhenium gasketed diamond anvil cell, equipped with a pair of diamonds with a 300 μm culet diameter. The ruby luminescence method was employed for pressure calibration.[29] The high-pressure XRD measurements at room temperature were performed at the 16BM-D beamline of the High Pressure Collaborative Access Team and the 13-BM-C beamline of the GeoSoilEnviroCARS (Geo Soil Enviro Consortium for Advanced Radiation Sources) at the Advanced Photon Source of Argonne National Laboratory.[30] The incident monochromatic X-ray beam energies were E = 28.6 keV (λ = 0.434 Å, $CuCr_2O_4$) and E = 29.2 keV (λ = 0.4246 Å, $CuCr_2Se_4$). The distances between the sample and diffraction imaging plate were 197.8 mm ($CuCr_2O_4$) and 328.35 mm ($CuCr_2Se_4$). The collected XRD diffractograms were processed with the FIT2D software.[31] Refinements were performed using the GSAS and EXPGUI software packages.[32,33] The P–V data were fitted with a Birch–Murnaghan equation of state (B–M EoS).[34] Helium served as a pressure-transmitting medium in all experiments.

3. RESULTS AND DISCUSSION

3.1. $CuCr_2O_4$ under Pressure. Overall, our high-pressure XRD study on $CuCr_2O_4$ reveals that the ambient-pressure $I4_1/amd$ structure is stable up to ∼50 GPa (Figure 2). The stability of the $I4_1/amd$ phase indicates the persistence of the Cu^{2+}-induced Jahn–Teller distortion up to 50 GPa. Such behavior is

DOI: 10.1021/acs.jpcc.7b04657
J. Phys. Chem. C 2017, 121, 16513−16520

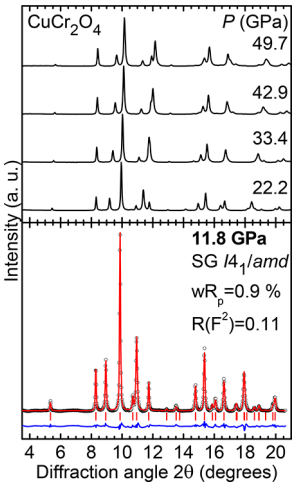

Figure 2. Selected XRD patterns of $CuCr_2O_4$ at various pressures (T = 300 K, λ = 0.434 Å). An example of a Rietveld refinement at 11.8 GPa is also shown (bottom). Dots stand for the measured spectra, the red solid line represents the best refinement, and their difference is drawn as a blue line. Vertical ticks mark the $I4_1/amd$ Bragg peak positions.

consistent with a recent high-pressure experimental study on $FeCr_2O_4$, which is shown to retain the pressure-induced Jahn–Teller active $I4_1/amd$ phase up to 74 GPa.[35] We note that the resilience of Jahn–Teller effects under compression is not the norm, since the effect of pressure is generally the suppression of Jahn–Teller distortions.[36,37]

Despite the persistence of the tetragonal phase, close inspection of the lattice parameters reveals a distinct change in the compressibility of the a-axis (Figure 3a). In particular, the pressure slope of the tetragonal a-axis increases above 23 GPa; i.e., the $I4_1/amd$ phase becomes more compressible in the a–b equatorial plane than the apical c-direction. No distinct compressibility changes could be observed either in the c-axis or in the bulk volume (Figure 3 a,b). Such an anomalous effect is observed for the first time in the Cr-bearing spinel family. A fitting of a second-order B–M EoS in the measured pressure–volume (P–V) data before and after 23 GPa yields bulk moduli values B_0 = 152(3) GPa and $B_{23\ GPa}$ = 240(5) GPa and their pressure derivatives B'_0 = 4.3(2) and $B'_{23\ GPa}$ = 4.2(6), respectively (Table 1), consistent with the respective values of $Fd\bar{3}m$ Cr-bearing oxide spinels.[11,38,35,39] We note though that a single B–M EoS could fit all of the P–V data.

Table 1. Elastic Parameters (Volume per Formula Unit V_R/Z, Bulk Modulus B_R, and Pressure Derivative of the Bulk Modulus B'_R) for Various Phases of $CuCr_2O_4$ and $CuCr_2Se_4$ under Pressure, As Obtained by the Fitting of the Birch–Murnaghan EoS Forms[34] to the Measured P–V Data[a]

compd	phase	P_R (GPa)	V_R/Z (Å^3)	B_R (GPa)	B'_R
$CuCr_2O_4$	$I4_1/amd$	10^{-4}	70.8 (exp)	152(3)	4.3(2)
	$I4_1/amd$	23	62.5 (exp)	240(5)	4.2(6)
$CuCr_2Se_4$	$Fd\bar{3}m$	10^{-4}	138.1 (exp)	82(5)	6(1)
	monoclinic	15	118.3 (exp)	108(1)	4 (fixed)

[a]Each parameter is evaluated at a reference pressure P_R. Exp = experimental value.

To gain a microscopic understanding of the mechanism behind this compressibility change, we have additionally plotted selected interatomic parameters, i.e., bond lengths and bond angles, as a function of pressure (Figure 3). The high quality of the measured XRD patterns allowed for full Rietveld refinements up to ~40 GPa; beyond that pressure point, only the lattice parameters were extracted (Table S1 in the Supporting Information). As we can observe in Figure 3c,d, only the apical Cr–O bond distances show a distinct anomaly in their pressure-induced behavior, as they expand beyond 23 GPa. Both the equatorial Cr–O and the tetrahedral Cu–O bond lengths decrease in almost linear fashion with increasing pressure (Figure 3). Given that the apical Cr–O bond length directly reflects the energetic configuration of the outer Cr^{3+} 3d orbitals along the z-direction,[4,40,41] such an increase of the apical bond distance implies an energetic downshift of the occupied $3d_{xz}$ and $3d_{yz}$ and the unoccupied $3d_{z^2}$ states and an

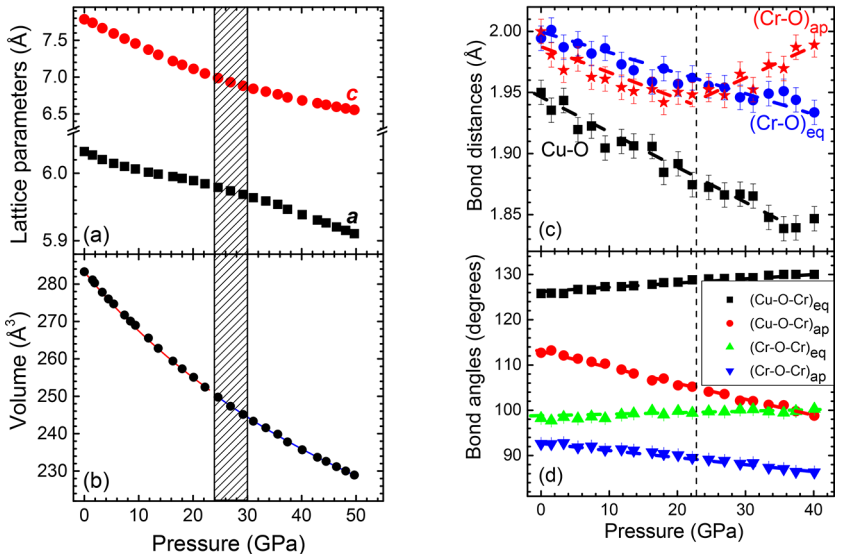

Figure 3. (a) Lattice constants, (b) unit cell volume, (c) selected interatomic bond lengths, and (d) bond angles of the $I4_1/amd$ phase of $CuCr_2O_4$ as a function of pressure. The red and blue solid lines going through the P–V data represent the fitted Birch–Murnaghan EoS functions before and after the isostructural transition, marked by vertical dashed lines (see the text). Error bars lie within the symbols in most cases.

DOI: 10.1021/acs.jpcc.7b04657
J. Phys. Chem. C 2017, 121, 16513–16520

energy increase of the occupied $3d_{xy}$ and unoccupied $3d_{x^2-y^2}$ orbitals above 23 GPa (Figure 4). Consequently, a Cr^{3+} 3d

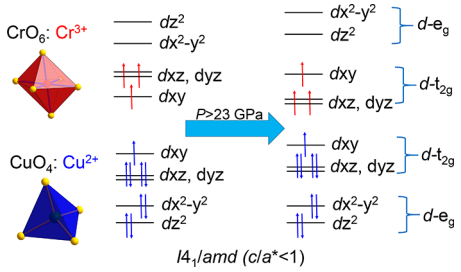

Figure 4. Schematic illustration of the outer 3d orbitals of the octahedrally coordinated Cr^{3+} and the tetrahedrally coordinated Cu^{2+} cations in the $I4_1/amd$ structure of $CuCr_2O_4$. Notice the orbital reorientation of the Cr^{3+} 3d states above 23 GPa, resulting from the expansion of the apical Cr−O bond lengths.

orbital reorientation might be the origin behind the observed compressibility anomaly in $CuCr_2O_4$ at 23 GPa. Interestingly, the $YTiO_3$ perovskite exhibits a similar behavior under pressure, which is demonstrated by an anomalous compressibility of specific Ti−O bond lengths.[42] More appropriate probes are needed, however, to unravel the exact origin behind this compressibility change.

Finally, the interatomic bond angles also show an almost linear variation upon compression (Figure 3d). We should remind here that the Cr−O−Cr bond angles serve as the pathways for indirect ferromagnetic exchange interactions, whereas the Cu−O−Cr bond angles modulate the antiferromagnetic interaction between the magnetic Cu and Cr cations.[43−45] As we can observe, the equatorial Cu−O−Cr and Cr−O−Cr bond angles do not show any appreciable change upon compression; i.e., they increase by 4° and 2° up to 40 GPa, respectively. On the other hand, their apical counterparts decrease in an almost doubled pressure rate, with the apical Cu−O−Cr bond angle exhibiting the largest variation (decrease by ∼15°).

3.2. $CuCr_2Se_4$ under Pressure. Contrary to $CuCr_2O_4$, $CuCr_2Se_4$ retains its starting $Fd\bar{3}m$ structure up to ∼8 GPa (Figure 5). Beyond that pressure, several new Bragg peaks appear in the XRD patterns, indicating a structural transition. This pressure-induced transformation is fully completed at about 20 GPa, showing sluggishness. Further compression appears to lead toward a high-symmetry disordered phase, as indicated by the relatively low number of observed XRD features and the emergence of an intense Bragg peak located at ∼9°. Such a transition, however, is not completed up to 45 GPa, the highest pressure achieved in our experiment.

Indexing of the observed XRD patterns above ∼20 GPa led to a monoclinic unit cell, which could reproduce all of the observed Bragg features (Figure 5b). Unfortunately, both the significant overlap of adjacent Bragg peaks (Figure 5b) and the development of high texture effects after the structural transformation hindered the determination of a unique space group and consequent Rietveld refinements; nevertheless, the extracted unit cell parameters matched the high-pressure modification of $ZnCr_2Se_4$;[13] i.e., $CuCr_2Se_4$ has apparently transformed into a $CrMo_2S_4$-type structure (SG Cc, $Z = 8$),[46] which in turn is a distorted variant of the Cr_3S_4-type phase.[47] In this structure, both the Cu and Cr cations exhibit 6-fold coordination with respect to the anions.

This $Fd\bar{3}m$ → monoclinic structural transition in $CuCr_2Se_4$ is really interesting for the structural systematics of Cr−selenide spinels under pressure, since, as we have shown in previous works,[12,14] the first pressure-induced structural transition of chalcogenide Cr spinels with nonmagnetic A cations appears to depend on the magnetic exchange interactions active in these systems; $ZnCr_2Se_4$, however, does not follow this trend.[12,14] $CuCr_2Se_4$ constitutes the second example of a Cr−selenide

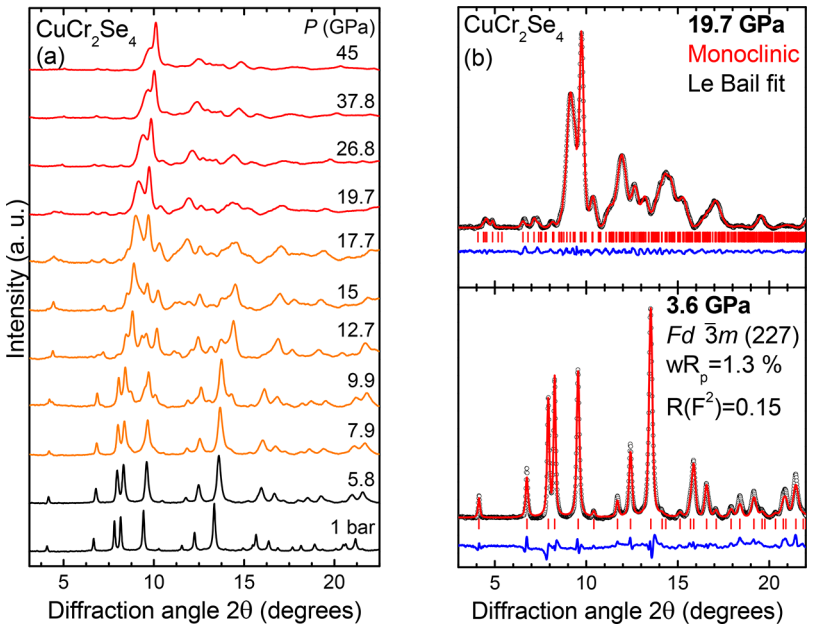

Figure 5. (a) Selected XRD patterns of $CuCr_2Se_4$ at various pressures (T = 300 K, λ = 0.4246 Å). The various phases are indicated by black ($Fd\bar{3}m$), red (monoclinic), and orange (phase mixture). (b) Refinements of $CuCr_2Se_4$ XRD patterns at 3.6 GPa (Rietveld, bottom) and at 19.7 GPa (Le Bail, top). Dots stand for the collected spectra, the red solid lines represent the best refinements, and their differences are drawn as blue lines. Vertical ticks mark the Bragg peak positions.

DOI: 10.1021/acs.jpcc.7b04657
J. Phys. Chem. C 2017, 121, 16513−16520

spinel adopting this complex monoclinic high-pressure phase after $ZnCr_2Se_4$, implying that the driving force behind this transformation is common in these two materials. We will come back to this point later in the Discussion.

In Figure 6 we present the experimental lattice parameters and the respective $P-V$ data of the $Fd\bar{3}m$ structure and the

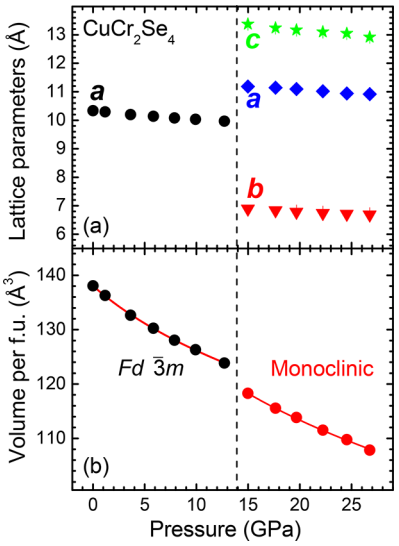

Figure 6. (a) Lattice constants and (b) unit cell volume per formula unit as a function of pressure for the various phases of $CuCr_2Se_4$. Error bars lie within the symbols. The vertical dashed line marks the onset pressure of the structural transition, whereas the red solid lines represent the fitted Birch–Murnaghan EoS functions.

monoclinic high-pressure phase of $CuCr_2Se_4$. The respective values are provided in Table S2 in the Supporting Information. We note that we could extract the lattice parameters of the monoclinic phase up to 27 GPa, as several low-intensity Bragg peaks either vanished or merged above that pressure, thus not allowing for meaningful refinements of the XRD patterns. As we can observe, the cubic–monoclinic transition exhibits a sizable volume decrease at the transition point (~4%), owing to the coordination increase of Cu with respect to Se from 4-fold to 6-fold. A similar volume drop at the transition point was also detected for $ZnCr_2Se_4$.[13]

The fitting of the $Fd\bar{3}m$ $P-V$ data with a third-order B–M EoS yielded a bulk modulus value of $B_0 = 82(5)$ GPa (Table 1), consistent with the calculated value[48] and consistent with the bulk moduli of relevant Cr–selenide spinels.[13,14,49] We note that the bulk modulus value of $CuCr_2Se_4$ is almost halved compared to $CuCr_2O_4$, owing to the larger size and the higher polarizability of the Se^{2-} with respect to the O^{2-} anions.[50] Furthermore, the bulk modulus value of the high-pressure monoclinic modification of $CuCr_2Se_4$ is comparable with the respective B value of the monoclinic $ZnCr_2Se_4$ high-pressure modification.[13]

Finally, we comment on the $CuCr_2Se_4$ XRD patterns above ~30 GPa. As we mentioned, the diminishing and the overlap of the Bragg features do not allow meaningful refinements above that pressure. Nevertheless, the diffractograms appear to evolve toward a structure with a smaller number of Bragg peaks, i.e., a high-symmetry phase (Figure 5a). A possible scenario might be that the high-pressure monoclinic phase $CdCr_2Se_4$ is transformed to a randomly disordered higher symmetry structure such as a cation-deficient NiAs-type phase or a CdI_2-type modification, a common high-pressure and high-temperature polymorph of several Cr thiospinels.[7,8,10,51,52]

3.3. Discussion. Comparison between the high-pressure behavior of $CuCr_2O_4$ and $CuCr_2Se_4$ can provide certain insights into the factors governing the pressure-induced structural behavior of Cr-bearing spinels.

As we mentioned earlier, the ternary ACr_2O_4 compounds (A = Mn–Zn, Cd, Hg) adopt the spinel structure at ambient conditions.[5] Even though there have not been many high-pressure studies in the literature, the reported investigations indicate that the high-pressure phase for the Cr-bearing oxide series is the tetragonal $I4_1/amd$ phase ($MgCr_2O_4$, $FeCr_2O_4$, and $CoCr_2O_4$),[35,38,39,53] which was attributed either to pressure-activated Jahn–Teller effects ($FeCr_2O_4$) or to variations in the magnetic exchange interactions ($CoCr_2O_4$). We note also that an unidentified orthorhombic phase has been reported for $ZnCr_2O_4$ above 30 GPa,[11] whereas infrared spectroscopic measurements indicated a transition of $CdCr_2O_4$ close to 15 GPa.[54] In light of these findings, it is not unusual that $CuCr_2O_4$ retains its starting $I4_1/amd$ structure up to ~50 GPa.

On the other hand, all of the ACr_2S_4 sulfides (A = Mn–Zn, Cd, Hg) crystallize in the spinel $Fd\bar{3}m$ structure at ambient conditions.[2] High-pressure and/or high-temperature treatment, however, transforms the spinel sulfides with magnetic A cations (Mn–Cu) into the denser Cr_3S_4-type phase;[8,9,55] this transition was not observed for $ZnCr_2S_4$ with nonmagnetic cations at the A site, as this material adopts the tetragonal $I4_1/amd$ structure under pressure.[12,56,57] This trend hints that the adoption of the Cr_3S_4-type phase is dependent on the outer electronic configuration of the A^{2+} cation. In other words, its adoption should be possible when the A^{2+} cations have unfilled 3d orbitals.

The aforementioned conclusion is further supported by the Cr-based selenide compounds. In particular, all of the ACr_2Se_4 members with magnetic A cations (A^{2+} = Mn–Ni) crystallize in the denser Cr_3S_4-type structure at ambient conditions already.[1] Compared with the respective sulfides, it appears that both the larger size and the more covalent character of Se^{2-} favor the adoption of this monoclinic structure for magnetic A cations. The latter implies that the chemical substitution of S^{2-} with Se^{2-} can be used to manipulate the structural as well as the rest of the physical properties in these systems.

Not all of the Cr-based selenides crystallize in the Cr_3S_4-type structure, however. $CuCr_2Se_4$, $ZnCr_2Se_4$, $CdCr_2Se_4$, and $HgCr_2Se_4$ adopt the spinel $Fd\bar{3}m$ phase.[44] We note that even though $CuCr_2Se_4$ also contains a magnetic cation at the A site, it does not adopt the Cr_3S_4-type structure at ambient conditions as the rest of the ACr_2Se_4 members with magnetic A cations. We tend to attribute this "inconsistency" to the valence state of Cu, as a significant portion of the Cu cations are in a monovalent valence state with their outer 3d orbitals fully occupied.[21] Nevertheless, compression of both $CuCr_2Se_4$ and $ZnCr_2Se_4$ induces transitions toward a $CrMo_2S_4$-type structure,[13] a superstructure of Cr_3S_4. The remaining Cr spinel selenides, i.e., $CdCr_2Se_4$ and $HgCr_2Se_4$, undergo transitions toward the tetragonal $I4_1/amd$ structure.[14,49] The respective $Fd\bar{3}m \rightarrow I4_1/amd$ transition pressures for both Cr-bearing sulfides and selenides were shown to be dependent on the ratio of magnetic exchange interactions of these systems.[12]

This trend is not followed by $ZnCr_2Se_4$, however, implying a different guiding force behind the $Fd\bar{3}m \rightarrow$ monoclinic structural transition for both $CuCr_2Se_4$ and $ZnCr_2Se_4$. Since the ionic radii of tetrahedrally coordinated Cu^{1+}, Cu^{2+}, and Zn^{2+}

DOI: 10.1021/acs.jpcc.7b04657
J. Phys. Chem. C 2017, 121, 16513–16520

are almost equivalent to that of 6-fold-coordinated Cr^{3+} [$r(Cu^{2+})$ = 0.57 Å, $r(Cu^{1+}) \equiv r(Zn^{2+})$ = 0.6 Å ≈ $r(Cr^{3+})$ = 0.615 Å],[58] it appears that the size similarity between the two types of cations facilitates the transformation toward a high-pressure structure, where both cations are octahedrally coordinated. In other words, it might be that *steric rather than magnetic/electronic effects* drive the $Fd\bar{3}m$ → monoclinic transition in these materials, i.e., the tendency of the cations to increase their coordination under pressure. An additional hint comes from the structural behavior of $CdCr_2Se_4$, which adopts a monoclinic Cr_3S_4-type superstructure under combined high-pressure and high-temperature treatment.[1] This result implies that the $Fd\bar{3}m$ → monoclinic transition may be a high-pressure polymorph for all selenide spinels owing most likely to the larger size and more covalent character of Se^{2-}, with its appearance taking place either at room temperature for cations of similar size or at higher temperatures for dissimilar cations, so as to overcome possible kinetic barriers.

4. CONCLUSIONS

In summary, our high-pressure XRD investigations on $CuCr_2O_4$ and $CuCr_2Se_4$ spinels revealed diverse structural behavior for the two compounds. On one hand, $CuCr_2O_4$ retains its ambient-pressure $I4_1/amd$ structure up to 50 GPa. Close inspection of the lattice and interatomic parameters reveals a compressibility change near 23 GPa, due to the expansion of the apical Cr−O bond distances. Considering a similar pressure-induced effect in $YTiO_3$ perovskite,[42] we speculate that an outer Cr^{3+} 3d orbital reorientation is taking place in $CuCr_2O_4$ near 23 GPa. Our suggestion needs to be checked, however, by appropriate experimental probes.

On the other hand, $CuCr_2Se_4$ undergoes a structural transformation from the starting $Fd\bar{3}m$ phase toward a monoclinic structure initiated at ∼8 GPa and completed at ∼20 GPa. The high-pressure behavior resembles that of $ZnCr_2Se_4$.[13] We speculate that, unlike similar chalcogenide Cr spinels,[12,14] it is mostly *steric effects* that are driving the $Fd\bar{3}m$ → monoclinic transition. Further compression above ∼30 GPa appears to induce a disordered high-symmetry modification, similar to the effects of combined high-pressure and high-temperature treatment on several Cr thiospinels.

■ ASSOCIATED CONTENT

Supporting Information

The Supporting Information is available free of charge on the ACS Publications website at DOI: 10.1021/acs.jpcc.7b04657.

Tables with the complete structural parameters for $CuCr_2O_4$ and the two phases of $CuCr_2Se_4$ under pressure (PDF)

■ AUTHOR INFORMATION

Corresponding Authors

*E-mail: ilias.efthymiopoulos@gfz-potsdam.
*E-mail: ywang235@oakland.edu.

ORCID

I. Efthimiopoulos: 0000-0001-6542-8188
Y. Wang: 0000-0001-6663-5912

Notes

The authors declare no competing financial interest.

■ ACKNOWLEDGMENTS

We acknowledge Dr. S. Tkachev at the GSECARS (GeoSoilEnviroCARS, Geo Soil Enviro Consortium for Advanced Radiation Sources) for his help with the DAC gas loading and Dr. D. Popov for his assistance with the XRD measurements. Portions of this work were performed at HPCAT (High Pressure Collaborative Access Team) (Sector 16), Advanced Photon Source (APS), Argonne National Laboratory. HPCAT operations are supported by the Department of Energy National Nuclear Security Administration (DOE-NNSA) under Award No. DE-NA0001974, with partial instrumentation funding by the National Science Foundation (NSF). Portions of this work were performed at GeoSoilEnviroCARS (The University of Chicago, Sector 13), APS, Argonne National Laboratory. GeoSoilEnviroCARS is supported by the National Science Foundation—Earth Sciences (Grant EAR-1128799) and Department of Energy—GeoSciences (Grant DE-FG02-94ER14466). Use of the Consortium for Materials Properties Research in Earth Sciences (COMPRES)/GSECARS gas loading system was supported by COMPRES under NSF Cooperative Agreement EAR 11-57758 and by GSECARS through NSF Grant EAR-1128799 and DOE Grant DE-FG02-94ER14466. This research used resources of the Advanced Photon Source, a U.S. DOE Office of Science User Facility operated for the DOE Office of Science by Argonne National Laboratory under Contract No. DE-AC02-06CH11357. We are grateful to the Michigan Space Grant Consortium and the Research Faculty Fellowship of Oakland University for supporting this research. This research has been partially supported by the Deutsche Forschungsgemeinschaft (DFG) via the Transregional Collaborative Research Center TRR 80 (Augsburg-Munich).

■ REFERENCES

(1) Banus, M. D.; Lavine, M. C. Polymorphism in Selenospinels- A High-Pressure Phase of $CdCr_2Se_4$. *J. Solid State Chem.* **1969**, *1*, 109−116.
(2) Rao, C. N. R.; Pisharody, K. P. R. Transition Metal Sulfides. *Prog. Solid State Chem.* **1976**, *10*, 207−270.
(3) Sickafus, K. E.; Wills, J. M.; Grimes, N. W. Structure of Spinel. *J. Am. Ceram. Soc.* **1999**, *82*, 3279−3292.
(4) Radaelli, P. G. Orbital Ordering in Transition-Metal Spinels. *New J. Phys.* **2005**, *7*, 53.
(5) Rao, C. N. R.; Raveau, B. *Transition Metal Oxides*, 2nd ed.; John Wiley & Sons Inc.: Hoboken, NJ, 1998.
(6) Rudolf, T.; Kant, C.; Mayr, F.; Hemberger, J.; Tsurkan, V.; Loidl, A. Spin-Phonon Coupling in Antiferromagnetic Chromium Spinels. *New J. Phys.* **2007**, *9*, 76.
(7) Bouchard, R. J. Spinel to Defect NiAs Structure Transformation. *Mater. Res. Bull.* **1967**, *2*, 459−464.
(8) Tressler, R. E.; Hummel, F. A.; Stubican, V. S. Pressure-Temperature Study of Sulfospinels. *J. Am. Ceram. Soc.* **1968**, *51*, 648−651.
(9) Amiel, Y.; Rozenberg, G. K.; Nissim, N.; Milner, A.; Pasternak, M. P.; Hanfland, M.; Taylor, R. D. Intricate Relationship between Pressure-Induced Electronic and Structural Transformations in $FeCr_2S_4$. *Phys. Rev. B: Condens. Matter Mater. Phys.* **2011**, *84*, 224114.
(10) Tressler, R. E.; Stubican, V. S. Magnetic Properties of $A^{2+}Cr_2S_4$ Compounds with the NiAs Structure. *J. Am. Ceram. Soc.* **1968**, *51*, 391−394.
(11) Levy, D.; Diella, V.; Pavese, A.; Dapiaggi, M.; Sani, A. P-V Equation of State, Thermal Expansion, and P-T Stability of Synthetic Zincochromite ($ZnCr_2O_4$ Spinel). *Am. Mineral.* **2005**, *90*, 1157−1162.

DOI: 10.1021/acs.jpcc.7b04657
J. Phys. Chem. C 2017, 121, 16513−16520

(12) Efthimiopoulos, I.; Lochbiler, T.; Tsurkan, V.; Loidl, A.; Felea, V.; Wang, Y. Structural Behavior of $ZnCr_2S_4$ Spinel Under Pressure. *J. Phys. Chem. C* **2017**, *121*, 769−777.
(13) Efthimiopoulos, I.; Liu, Z. T. Y.; Khare, S. V.; Sarin, P.; Tsurkan, V.; Loidl, A.; Popov, D.; Wang, Y. Structural Transition in the Magnetoelectric $ZnCr_2Se_4$ Spinel under Pressure. *Phys. Rev. B: Condens. Matter Mater. Phys.* **2016**, *93*, 174103.
(14) Efthimiopoulos, I.; Liu, Z. T. Y.; Kucway, M.; Khare, S. V.; Sarin, P.; Tsurkan, V.; Loidl, A.; Wang, Y. Pressure-Induced Phase Transitions in the $CdCr_2Se_4$ Spinel. *Phys. Rev. B: Condens. Matter Mater. Phys.* **2016**, *94*, 174106.
(15) Iwata-Harms, J. M.; Wong, F. J.; Alaan, U. S.; Kirby, B. J.; Borchers, J. A.; Toney, M. F.; Nelson-Cheeseman, B. B.; Liberati, M.; Arenholz, E.; Suzuki, Y. Controlling Spin Ordering in Frustrated Magnets via Thin Film Heteroepitaxy. *Phys. Rev. B: Condens. Matter Mater. Phys.* **2012**, *85*, 214424.
(16) Dollase, W. A.; O'Neill, H. S. C. The Spinels $CuCr_2O_4$ and $CuRh_2O_4$. *Acta Crystallogr., Sect. C: Cryst. Struct. Commun.* **1997**, *53*, 657−659.
(17) Kennedy, B. J.; Zhou, Q. The Role of Orbital Ordering in the Tetragonal-to-Cubic Phase Transition in $CuCr_2O_4$. *J. Solid State Chem.* **2008**, *181*, 2227−2230.
(18) Bordacs, S.; Varjas, D.; Kezsmarki, I.; Mihaly, G.; Baldassarre, L.; Abouelsayed, A.; Kuntscher, C. A.; Ohgushi, K.; Tokura, Y. Magnetic-Order-Induced Crystal Symmetry Lowering in ACr_2O_4 Ferrimagnetic Spinels. *Phys. Rev. Lett.* **2009**, *103*, 077205.
(19) Prince, E. Crystal and Magnetic Structure of Copper Chromite. *Acta Crystallogr.* **1957**, *10*, 554−556.
(20) Suchomel, M. R.; Shoemaker, D. P.; Ribaud, L.; Kemei, M. C.; Seshadri, R. Spin-Induced Symmetry Breaking in Orbitally Ordered $NiCr_2O_4$ and $CuCr_2O_4$. *Phys. Rev. B: Condens. Matter Mater. Phys.* **2012**, *86*, 054406.
(21) Noh, H.-J.; Kang, J.-S.; Lee, S. S.; Kim, G.; Han, S.-W.; Oh, S.-J.; Kim, J.-Y.; Lee, H.-G.; Yeo, S.; Guha, S.; et al. Valence Values of the Cations in Selenospinel $Cu(Cr, Ti)_2Se_4$. *Eur. Phys. Lett.* **2007**, *78*, 27004.
(22) Zhang, L.; Ling, L.; Fan, J.; Li, R.; Tan, S.; Zhang, Y. 3D-Heisenberg Ferromagnetic Characteristics in $CuCr_2Se_4$. *J. Appl. Phys.* **2011**, *109*, 113911.
(23) Saha-Dasgupta, T.; De Raychaudhury, M.; Sarma, D. D. Ferromagnetism in Metallic Chalcospinels $CuCr_2S_4$ and $CuCr_2Se_4$. *Phys. Rev. B: Condens. Matter Mater. Phys.* **2007**, *76*, 054441.
(24) Kanomata, T.; Ido, H.; Kaneko, T. Effect of Pressure on Curie Temperatures of Chalcogenide Spinels $CuCr_2X_4$ (X = S, Se and Te). *J. Phys. Soc. Jpn.* **1970**, *29*, 332−335.
(25) Bettinger, J. S.; Chopdekar, R. V.; Liberati, M.; Neulinger, J. R.; Chshiev, M.; Takamura, Y.; Alldredge, L. M. B.; Arenholz, E.; Idzerda, Y. U.; Stacy, A. M.; et al. Magnetism and Transport of $CuCr_2Se_4$ Thin Films. *J. Magn. Magn. Mater.* **2007**, *318*, 65−73.
(26) Tamura, S. Pressure Effects on the Curie-Temperature of Spinel-Type $NiMn_2O_4$ and $CuCr_2O_4$. *J. Phys. Chem. Solids* **1994**, *55*, 461−464.
(27) Alvaro, M.; Nestola, F.; Ross, N.; Domeneghetti, M. C.; Reznitsky, L. High-Pressure Behavior of Thiospinel $CuCr_2S_4$. *Am. Mineral.* **2014**, *99*, 908−913.
(28) Dmitrieva, T. V.; Lyubutin, I. S.; Stepin, A. S.; Dubinskaya, Y. L.; Smirnovskaya, E. M.; Berry, F. J.; Thomas, M. F. Diamagnetic Nuclear 119 Sn Probes in the Copper Chromites $CuCr_2X_4$ (X = O, S, Se) with a Spinel Structure. *J. Exp. Theor. Phys.* **2007**, *104*, 554−561.
(29) Syassen, K. Ruby under Pressure. *High Pressure Res.* **2008**, *28*, 75−126.
(30) Zhang, D.; Dera, P. K.; Eng, P. J.; Stubbs, J. E.; Zhang, J. S.; Prakapenka, V. B.; Rivers, M. L. High Pressure Single Crystal Diffraction at PX̂2. *J. Visualized Exp.* **2017**, *119*, e54660.
(31) Hammersley, A.; Svensson, S.; Hanfland, M.; Fitch, A.; Hausermann, D. Two-dimensional detector software: From real detector to idealised image or two-theta scan. *High Pressure Res.* **1996**, *14*, 235−248.
(32) Toby, B. H. EXPGUI, a Graphical User Interface for GSAS. *J. Appl. Crystallogr.* **2001**, *34*, 210−213.
(33) von Dreele, R. B.; Larson, A. C. *GSAS*; Los Alamos National Laboratory Report No. LAUR 86−748; Los Alamos, NM, 1994.
(34) Birch, F. Finite Elastic Strain of Cubic Crystals. *Phys. Rev.* **1947**, *71*, 809−824.
(35) Xu, W. M.; Hearne, G. R.; Layek, S.; Levy, D.; Itie, J.-P.; Pasternak, M. P.; Rozenberg, G. K.; Greenberg, E. $FeCr_2O_4$ Spinel to near Megabar Pressures: Orbital Moment Collapse and Site-Inversion Facilitated Spin Crossover. *Phys. Rev. B: Condens. Matter Mater. Phys.* **2017**, *95*, 045110.
(36) Loa, I.; Adler, P.; Grzechnik, A.; Syassen, K.; Schwarz, U.; Hanfland, M.; Rozenberg, G. K.; Gorodetsky, P.; Pasternak, M. P. Pressure-Induced Quenching of the Jahn-Teller Distortion and Insulator-to-Metal Transition in $LaMnO_3$. *Phys. Rev. Lett.* **2001**, *87*, 125501.
(37) Ruiz-Fuertes, J.; Segura, A.; Rodriguez, F.; Errandonea, D.; Sanz-Ortiz, M. N. Anomalous High-Pressure Jahn-Teller Behavior in $CuWO_4$. *Phys. Rev. Lett.* **2012**, *108*, 166402.
(38) Efthimiopoulos, I.; Liu, Z. T.; Khare, S. V.; Sarin, P.; Lochbiler, T.; Tsurkan, V.; Loidl, A.; Popov, D.; Wang, Y. Pressure-Induced Transition in the Multiferroic $CoCr_2O_4$ Spinel. *Phys. Rev. B: Condens. Matter Mater. Phys.* **2015**, *92*, 064108.
(39) Kyono, A.; Gramsch, S. A.; Yamanaka, T.; Ikuta, D.; Ahart, M.; Mysen, B. O.; Mao, H. K.; Hemley, R. J. The Influence of the Jahn-Teller Effect at Fe^{2+} on the Structure of Chromite at High Pressure. *Phys. Chem. Miner.* **2012**, *39*, 131−141.
(40) Dunitz, J. D.; Orgel, L. E. Electronic Properties of Transition-Metal Oxides I: Distortions from Cubic Symmetry. *J. Phys. Chem. Solids* **1957**, *3*, 20−29.
(41) Goodenough, J. B. Direct Cation-Cation Interactions in Several Oxides. *Phys. Rev.* **1960**, *117*, 1442−1451.
(42) Loa, I.; Wang, X.; Syassen, K.; Roth, H.; Lorenz, T.; Hanfland, M.; Mathis, Y.-L. Crystal Structure and the Mott-Hubbard Gap in $YTiO_3$ at High Pressure. *J. Phys.: Condens. Matter* **2007**, *19*, 406223.
(43) Das, D.; Ghosh, S. Density Functional Theory Based Comparative Study of Electronic Structures and Magnetic Properties of Spinel ACr_2O_4 (A = Mn, Fe, Co, Ni) Compounds. *J. Phys. D: Appl. Phys.* **2015**, *48*, 425001.
(44) Baltzer, P. K.; Wojtowicz, P. J.; Robbins, M.; Lopatin, E. Exchange Interactions in FM Cr Chalcogenide Spinels. *Phys. Rev.* **1966**, *151*, 367−377.
(45) Yaresko, A. N. Electronic Band Structure and Exchange Coupling Constants in ACr_2X_4 Spinels (A = Zn, Cd, Hg; X = O, S, Se). *Phys. Rev. B: Condens. Matter Mater. Phys.* **2008**, *77*, 115106.
(46) Vaqueiro, P.; Kosidowski, M. L.; Powell, A. V. Structural Distortions of the Metal Dichalcogenide Units in AMo_2S_4 (A = V, Cr, Fe, Co) and Magnetic and Electrical Properties. *Chem. Mater.* **2002**, *14*, 1201−1209.
(47) Guillevic, P. J.; Le Marouille, J.-Y.; Grandjean, D. Etude Structurale de Combinaisons Sulfurees et Seleniees Du Molybdene. IV. Structures Cristallines de $CoMo_2S_4$ et de $FeMo_2S_4$. *Acta Crystallogr., Sect. B: Struct. Crystallogr. Cryst. Chem.* **1974**, *B30*, 111−117.
(48) Waskowska, A.; Gerward, L.; Olsen, J. S.; Marques, M.; Contreras-Garcia, J.; Recio, J. M. The Bulk Modulus of Cubic Spinel Selenides: An Experimental and Theoretical Study. *High Pressure Res.* **2009**, *29*, 72−75.
(49) Efthimiopoulos, I.; Yaresko, A.; Tsurkan, V.; Deisenhofer, J.; Loidl, A.; Park, C.; Wang, Y. Pressurizing the $HgCr_2Se_4$ Spinel at Room Temperature. *Appl. Phys. Lett.* **2014**, *104*, 011911.
(50) Waskowska, A.; Gerward, L.; Olsen, J. S.; Feliz, M.; Llusar, R.; Gracia, L.; Marques, M.; Recio, J. M. High-Pressure Behaviour of Selenium-Based Spinels and Related Structures-an Experimental and Theoretical Study. *J. Phys.: Condens. Matter* **2004**, *16*, 53−63.
(51) Vaqueiro, P.; Powell, A. V.; Hull, S.; Keen, D. A. Pressure-Induced Phase Transitions in Chromium Thiospinels. *Phys. Rev. B: Condens. Matter Mater. Phys.* **2001**, *63*, 064106.

DOI: 10.1021/acs.jpcc.7b04657
J. Phys. Chem. C 2017, 121, 16513−16520

(52) Vaqueiro, P.; Powell, A. V.; Lebech, B. Order-Disorder Transitions in $NiCr_2S_4$. *Physica B* **2000**, *276−278*, 238−239.
(53) Yong, W.; Botis, S.; Shieh, S. R.; Shi, W.; Withers, A. C. Pressure-Induced Phase Transition Study of Magnesiochromite ($MgCr_2O_4$) by Raman Spectroscopy and X-Ray Diffraction. *Phys. Earth Planet. Inter.* **2012**, *196−197*, 75−82.
(54) Rabia, K.; Baldassarre, L.; Deisenhofer, J.; Tsurkan, V.; Kuntscher, C. A. Evolution of the Optical Properties of Chromium Spinels $CdCr_2O_4$, $HgCr_2S_4$, and $ZnCr_2Se_4$ under High Pressure. *Phys. Rev. B: Condens. Matter Mater. Phys.* **2014**, *89*, 125107.
(55) Albers, W.; Rooymans, C. J. M. High Pressure Polymorphism of Spinel Compounds. *Solid State Commun.* **1965**, *3*, 417−419.
(56) Efthimiopoulos, I.; Yaresko, A.; Tsurkan, V.; Deisenhofer, J.; Loidl, A.; Park, C.; Wang, Y. Multiple Pressure-Induced Transitions in $HgCr_2S_4$. *Appl. Phys. Lett.* **2013**, *103*, 201908.
(57) Efthimiopoulos, I. High-Pressure Structural and Spectroscopic Studies on Transition Metal Compounds. Doctoral Thesis, Aristotle University of Thessaloniki, 2010.
(58) Shannon, R. D.; Prewitt, C. T. Effective Ionic Radii in Oxides and Fluorides. *Acta Crystallogr., Sect. B: Struct. Crystallogr. Cryst. Chem.* **1969**, *25*, 925−946.

DOI: 10.1021/acs.jpcc.7b04657
J. Phys. Chem. C 2017, 121, 16513−16520